

First Observation of $D^+ \rightarrow \eta\mu^+\nu_\mu$ and Measurement of its Decay Dynamics

M. Ablikim¹, M. N. Achasov^{10,c}, P. Adlarson⁶⁴, S. Ahmed¹⁵, M. Albrecht⁴, A. Amoroso^{63A,63C}, Q. An^{60,48}, Anita²¹, X. H. Bai⁵⁴, Y. Bai⁴⁷, O. Bakina²⁹, R. Baldini Ferroli^{23A}, I. Balossino^{24A}, Y. Ban^{38,k}, K. Begzsuren²⁶, J. V. Bennett⁵, N. Berger²⁸, M. Bertani^{23A}, D. Bettoni^{24A}, F. Bianchi^{63A,63C}, J. Biernat⁶⁴, J. Bloms⁵⁷, A. Bortone^{63A,63C}, I. Boyko²⁹, R. A. Briere⁵, H. Cai⁶⁵, X. Cai^{1,48}, A. Calcaterra^{23A}, G. F. Cao^{1,52}, N. Cao^{1,52}, S. A. Cetin^{51B}, J. F. Chang^{1,48}, W. L. Chang^{1,52}, G. Chelkov^{29,b}, D. Y. Chen⁶, G. Chen¹, H. S. Chen^{1,52}, M. L. Chen^{1,48}, S. J. Chen³⁶, X. R. Chen²⁵, Y. B. Chen^{1,48}, W. S. Cheng^{63C}, G. Cibinetto^{24A}, F. Cossio^{63C}, X. F. Cui³⁷, H. L. Dai^{1,48}, J. P. Dai^{42,g}, X. C. Dai^{1,52}, A. Dbeyssi¹⁵, R. B. de Boer⁴, D. Dedovich²⁹, Z. Y. Deng¹, A. Denig²⁸, I. Denysenko²⁹, M. Destefanis^{63A,63C}, F. De Mori^{63A,63C}, Y. Ding³⁴, C. Dong³⁷, J. Dong^{1,48}, L. Y. Dong^{1,52}, M. Y. Dong^{1,48,52}, S. X. Du⁶⁸, J. Fang^{1,48}, S. S. Fang^{1,52}, Y. Fang¹, R. Farinelli^{24A}, L. Fava^{63B,63C}, F. Feldbauer⁴, G. Felici^{23A}, C. Q. Feng^{60,48}, M. Fritsch⁴, C. D. Fu¹, Y. Fu¹, X. L. Gao^{60,48}, Y. Gao^{38,k}, Y. Gao⁶¹, Y. G. Gao⁶, I. Garzia^{24A,24B}, E. M. Gersabeck⁵⁵, A. Gilman⁵⁶, K. Goetzen¹¹, L. Gong³⁷, W. X. Gong^{1,48}, W. Gradl²⁸, M. Greco^{63A,63C}, L. M. Gu³⁶, M. H. Gu^{1,48}, S. Gu², Y. T. Gu¹³, C. Y. Guan^{1,52}, A. Q. Guo²², L. B. Guo³⁵, R. P. Guo⁴⁰, Y. P. Guo^{9,h}, Y. P. Guo²⁸, A. Guskov²⁹, S. Han⁶⁵, T. T. Han⁴¹, T. Z. Han^{9,h}, X. Q. Hao¹⁶, F. A. Harris⁵³, K. L. He^{1,52}, F. H. Heinsius⁴, T. Held⁴, Y. K. Heng^{1,48,52}, M. Himmelreich^{11,f}, T. Holtmann⁴, Y. R. Hou⁵², Z. L. Hou¹, H. M. Hu^{1,52}, J. F. Hu^{42,g}, T. Hu^{1,48,52}, Y. Hu¹, G. S. Huang^{60,48}, L. Q. Huang⁶¹, X. T. Huang⁴¹, Y. P. Huang¹, Z. Huang^{38,k}, N. Huesken⁵⁷, T. Hussain⁶², W. Ikegami Andersson⁶⁴, W. Imoehl²², M. Irshad^{60,48}, S. Jaeger⁴, S. Janchiv^{26,j}, Q. Ji¹, Q. P. Ji¹⁶, X. B. Ji^{1,52}, X. L. Ji^{1,48}, H. B. Jiang⁴¹, X. S. Jiang^{1,48,52}, X. Y. Jiang³⁷, J. B. Jiao⁴¹, Z. Jiao¹⁸, S. Jin³⁶, Y. Jin⁵⁴, T. Johansson⁶⁴, N. Kalantar-Nayestanaki³¹, X. S. Kang³⁴, R. Kappert³¹, M. Kavatsyuk³¹, B. C. Ke^{43,1}, I. K. Keshk⁴, A. Khoukaz⁵⁷, P. Kiese²⁸, R. Kiuchi¹, R. Kliemt¹¹, L. Koch³⁰, O. B. Kolcu^{51B,e}, B. Kopf⁴, M. Kuemmel⁴, M. Kuessner⁴, A. Kupsc⁶⁴, M. G. Kurth^{1,52}, W. Kühn³⁰, J. J. Lane⁵⁵, J. S. Lange³⁰, P. Larin¹⁵, L. Lavezzi^{63C}, H. Leithoff²⁸, M. Lellmann²⁸, T. Lenz²⁸, C. Li³⁹, C. H. Li³³, Cheng Li^{60,48}, D. M. Li⁶⁸, F. Li^{1,48}, G. Li¹, H. B. Li^{1,52}, H. J. Li^{9,h}, J. L. Li⁴¹, J. Q. Li⁴, Ke Li¹, L. K. Li¹, Lei Li³, P. L. Li^{60,48}, P. R. Li³², S. Y. Li⁵⁰, W. D. Li^{1,52}, W. G. Li¹, X. H. Li^{60,48}, X. L. Li⁴¹, Z. B. Li⁴⁹, Z. Y. Li⁴⁹, H. Liang^{60,48}, H. Liang^{1,52}, Y. F. Liang⁴⁵, Y. T. Liang²⁵, L. Z. Liao^{1,52}, J. Libby²¹, C. X. Lin⁴⁹, B. Liu^{42,g}, B. J. Liu¹, C. X. Liu¹, D. Liu^{60,48}, D. Y. Liu^{42,g}, F. H. Liu⁴⁴, Fang Liu¹, Feng Liu⁶, H. B. Liu¹³, H. M. Liu^{1,52}, Huanhuan Liu¹, Huihui Liu¹⁷, J. B. Liu^{60,48}, J. Y. Liu^{1,52}, K. Liu¹, K. Y. Liu³⁴, Ke Liu⁶, L. Liu^{60,48}, Q. Liu⁵², S. B. Liu^{60,48}, Shuai Liu⁴⁶, T. Liu^{1,52}, X. Liu³², Y. B. Liu³⁷, Z. A. Liu^{1,48,52}, Z. Q. Liu⁴¹, Y. F. Long^{38,k}, X. C. Lou^{1,48,52}, F. X. Lu¹⁶, H. J. Lu¹⁸, J. D. Lu^{1,52}, J. G. Lu^{1,48}, X. L. Lu¹, Y. Lu¹, Y. P. Lu^{1,48}, C. L. Luo³⁵, M. X. Luo⁶⁷, P. W. Luo⁴⁹, T. Luo^{9,h}, X. L. Luo^{1,48}, S. Lusso^{63C}, X. R. Lyu⁵², F. C. Ma³⁴, H. L. Ma¹, L. L. Ma⁴¹, M. M. Ma^{1,52}, Q. M. Ma¹, R. Q. Ma^{1,52}, R. T. Ma⁵², X. N. Ma³⁷, X. X. Ma^{1,52}, X. Y. Ma^{1,48}, Y. M. Ma⁴¹, F. E. Maas¹⁵, M. Maggiora^{63A,63C}, S. Maldaner²⁸, S. Malde⁵⁸, Q. A. Malik⁶², A. Mangoni^{23B}, Y. J. Mao^{38,k}, Z. P. Mao¹, S. Marcello^{63A,63C}, Z. X. Meng⁵⁴, J. G. Messchendorp³¹, G. Mezzadri^{24A}, T. J. Min³⁶, R. E. Mitchell²², X. H. Mo^{1,48,52}, Y. J. Mo⁶, N. Yu. Muchnoi^{10,c}, H. Muramatsu⁵⁶, S. Nakhoul^{11,f}, Y. Nefedov²⁹, F. Nerling^{11,f}, I. B. Nikolaev^{10,c}, Z. Ning^{1,48}, S. Nisar^{8,i}, S. L. Olsen⁵², Q. Ouyang^{1,48,52}, S. Pacetti^{23B,23C}, X. Pan^{9,h}, Y. Pan⁵⁵, A. Pathak¹, P. Patteri^{23A}, M. Pelizaeus⁴, H. P. Peng^{60,48}, K. Peters^{11,f}, J. Pettersson⁶⁴, J. L. Ping³⁵, R. G. Ping^{1,52}, A. Pitka⁴, R. Poling⁵⁶, V. Prasad^{60,48}, H. Qi^{60,48}, H. R. Qi⁵⁰, M. Qi³⁶, T. Y. Qi⁹, T. Y. Qi², S. Qian^{1,48}, W.-B. Qian⁵², Z. Qian⁴⁹, C. F. Qiao⁵², L. Q. Qin¹², X. P. Qin¹³, X. S. Qin⁴, Z. H. Qin^{1,48}, J. F. Qiu¹, S. Q. Qu³⁷, K. H. Rashid⁶², K. Ravindran²¹, C. F. Redmer²⁸, A. Rivetti^{63C}, V. Rodin³¹, M. Rolo^{63C}, G. Rong^{1,52}, Ch. Rosner¹⁵, M. Rump⁵⁷, A. Sarantsev^{29,d}, Y. Schelhaas²⁸, C. Schnier⁴, K. Schoenning⁶⁴, D. C. Shan⁴⁶, W. Shan¹⁹, X. Y. Shan^{60,48}, M. Shao^{60,48}, C. P. Shen⁹, P. X. Shen³⁷, X. Y. Shen^{1,52}, H. C. Shi^{60,48}, R. S. Shi^{1,52}, X. Shi^{1,48}, X. D. Shi^{60,48}, J. J. Song⁴¹, Q. Q. Song^{60,48}, W. M. Song^{27,1}, Y. X. Song^{38,k}, S. Sosio^{63A,63C}, S. Spataro^{63A,63C}, F. F. Sui⁴¹, G. X. Sun¹, J. F. Sun¹⁶, L. Sun⁶⁵, S. S. Sun^{1,52}, T. Sun^{1,52}, W. Y. Sun³⁵, Y. J. Sun^{60,48}, Y. K. Sun^{60,48}, Y. Z. Sun¹, Z. T. Sun¹, Y. H. Tan⁶⁵, Y. X. Tan^{60,48}, C. J. Tang⁴⁵, G. Y. Tang¹, J. Tang⁴⁹, V. Thoren⁶⁴, B. Tsednee²⁶, I. Uman^{51D}, B. Wang¹, B. L. Wang⁵², C. W. Wang³⁶, D. Y. Wang^{38,k}, H. P. Wang^{1,52}, K. Wang^{1,48}, L. L. Wang¹, M. Wang⁴¹, M. Z. Wang^{38,k}, Meng Wang^{1,52}, W. H. Wang⁶⁵, W. P. Wang^{60,48}, X. Wang^{38,k}, X. F. Wang³², X. L. Wang^{9,h}, Y. Wang⁴⁹, Y. Wang^{60,48}, Y. D. Wang¹⁵, Y. F. Wang^{1,48,52}, Y. Q. Wang¹, Z. Wang^{1,48}, Z. Y. Wang¹, Ziyi Wang⁵², Zongyuan Wang^{1,52}, D. H. Wei¹², P. Weidenkaff²⁸, F. Weidner⁵⁷, S. P. Wen¹, D. J. White⁵⁵, U. Wiedner⁴, G. Wilkinson⁵⁸, M. Wolke⁶⁴, L. Wollenberg⁴, J. F. Wu^{1,52}, L. H. Wu¹, L. J. Wu^{1,52}, X. Wu^{9,h}, Z. Wu^{1,48}, L. Xia^{60,48}, H. Xiao^{9,h}, S. Y. Xiao¹, Y. J. Xiao^{1,52}, Z. J. Xiao³⁵, X. H. Xie^{38,k}, Y. G. Xie^{1,48}, Y. H. Xie⁶,

T. Y. Xing^{1,52}, X. A. Xiong^{1,52}, G. F. Xu¹, J. J. Xu³⁶, Q. J. Xu¹⁴, W. Xu^{1,52}, X. P. Xu⁴⁶, F. Yan^{9,h}, L. Yan^{9,h}, L. Yan^{63A,63C}, W. B. Yan^{60,48}, W. C. Yan⁶⁸, Xu Yan⁴⁶, H. J. Yang^{42,g}, H. X. Yang¹, L. Yang⁶⁵, R. X. Yang^{60,48}, S. L. Yang^{1,52}, Y. H. Yang³⁶, Y. X. Yang¹², Yifan Yang^{1,52}, Zhi Yang²⁵, M. Ye^{1,48}, M. H. Ye⁷, J. H. Yin¹, Z. Y. You⁴⁹, B. X. Yu^{1,48,52}, C. X. Yu³⁷, G. Yu^{1,52}, J. S. Yu^{20,l}, T. Yu⁶¹, C. Z. Yuan^{1,52}, W. Yuan^{63A,63C}, X. Q. Yuan^{38,k}, Y. Yuan¹, Z. Y. Yuan⁴⁹, C. X. Yue³³, A. Yuncu^{51B,a}, A. A. Zafar⁶², Y. Zeng^{20,l}, B. X. Zhang¹, Guangyi Zhang¹⁶, H. H. Zhang⁴⁹, H. Y. Zhang^{1,48}, J. L. Zhang⁶⁶, J. Q. Zhang⁴, J. W. Zhang^{1,48,52}, J. Y. Zhang¹, J. Z. Zhang^{1,52}, Jianyu Zhang^{1,52}, Jiawei Zhang^{1,52}, L. Zhang¹, Lei Zhang³⁶, S. Zhang⁴⁹, S. F. Zhang³⁶, T. J. Zhang^{42,g}, X. Y. Zhang⁴¹, Y. Zhang⁵⁸, Y. H. Zhang^{1,48}, Y. T. Zhang^{60,48}, Yan Zhang^{60,48}, Yao Zhang¹, Yi Zhang^{9,h}, Z. H. Zhang⁶, Z. Y. Zhang⁶⁵, G. Zhao¹, J. Zhao³³, J. Y. Zhao^{1,52}, J. Z. Zhao^{1,48}, Lei Zhao^{60,48}, Ling Zhao¹, M. G. Zhao³⁷, Q. Zhao¹, S. J. Zhao⁶⁸, Y. B. Zhao^{1,48}, Y. X. Zhao²⁵, Z. G. Zhao^{60,48}, A. Zhemchugov^{29,b}, B. Zheng⁶¹, J. P. Zheng^{1,48}, Y. Zheng^{38,k}, Y. H. Zheng⁵², B. Zhong³⁵, C. Zhong⁶¹, L. P. Zhou^{1,52}, Q. Zhou^{1,52}, X. Zhou⁶⁵, X. K. Zhou⁵², X. R. Zhou^{60,48}, A. N. Zhu^{1,52}, J. Zhu³⁷, K. Zhu¹, K. J. Zhu^{1,48,52}, S. H. Zhu⁵⁹, W. J. Zhu³⁷, X. L. Zhu⁵⁰, Y. C. Zhu^{60,48}, Z. A. Zhu^{1,52}, B. S. Zou¹, J. H. Zou¹

(BESIII Collaboration)

- ¹ *Institute of High Energy Physics, Beijing 100049, People's Republic of China*
² *Beihang University, Beijing 100191, People's Republic of China*
³ *Beijing Institute of Petrochemical Technology, Beijing 102617, People's Republic of China*
⁴ *Bochum Ruhr-University, D-44780 Bochum, Germany*
⁵ *Carnegie Mellon University, Pittsburgh, Pennsylvania 15213, USA*
⁶ *Central China Normal University, Wuhan 430079, People's Republic of China*
⁷ *China Center of Advanced Science and Technology, Beijing 100190, People's Republic of China*
⁸ *COMSATS University Islamabad, Lahore Campus, Defence Road, Off Raiwind Road, 54000 Lahore, Pakistan*
⁹ *Fudan University, Shanghai 200443, People's Republic of China*
¹⁰ *G.I. Budker Institute of Nuclear Physics SB RAS (BINP), Novosibirsk 630090, Russia*
¹¹ *GSI Helmholtzcentre for Heavy Ion Research GmbH, D-64291 Darmstadt, Germany*
¹² *Guangxi Normal University, Guilin 541004, People's Republic of China*
¹³ *Guangxi University, Nanning 530004, People's Republic of China*
¹⁴ *Hangzhou Normal University, Hangzhou 310036, People's Republic of China*
¹⁵ *Helmholtz Institute Mainz, Johann-Joachim-Becher-Weg 45, D-55099 Mainz, Germany*
¹⁶ *Henan Normal University, Xinxiang 453007, People's Republic of China*
¹⁷ *Henan University of Science and Technology, Luoyang 471003, People's Republic of China*
¹⁸ *Huangshan College, Huangshan 245000, People's Republic of China*
¹⁹ *Hunan Normal University, Changsha 410081, People's Republic of China*
²⁰ *Hunan University, Changsha 410082, People's Republic of China*
²¹ *Indian Institute of Technology Madras, Chennai 600036, India*
²² *Indiana University, Bloomington, Indiana 47405, USA*
²³ *(A)INFN Laboratori Nazionali di Frascati, I-00044, Frascati, Italy; (B)INFN Sezione di Perugia, I-06100, Perugia, Italy; (C)University of Perugia, I-06100, Perugia, Italy*
²⁴ *(A)INFN Sezione di Ferrara, I-44122, Ferrara, Italy; (B)University of Ferrara, I-44122, Ferrara, Italy*
²⁵ *Institute of Modern Physics, Lanzhou 730000, People's Republic of China*
²⁶ *Institute of Physics and Technology, Peace Ave. 54B, Ulaanbaatar 13330, Mongolia*
²⁷ *Jilin University, Changchun 130012, People's Republic of China*
²⁸ *Johannes Gutenberg University of Mainz, Johann-Joachim-Becher-Weg 45, D-55099 Mainz, Germany*
²⁹ *Joint Institute for Nuclear Research, 141980 Dubna, Moscow region, Russia*
³⁰ *Justus-Liebig-Universitaet Giessen, II. Physikalisches Institut, Heinrich-Buff-Ring 16, D-35392 Giessen, Germany*
³¹ *KVI-CART, University of Groningen, NL-9747 AA Groningen, The Netherlands*
³² *Lanzhou University, Lanzhou 730000, People's Republic of China*
³³ *Liaoning Normal University, Dalian 116029, People's Republic of China*
³⁴ *Liaoning University, Shenyang 110036, People's Republic of China*
³⁵ *Nanjing Normal University, Nanjing 210023, People's Republic of China*
³⁶ *Nanjing University, Nanjing 210093, People's Republic of China*

- ³⁷ Nankai University, Tianjin 300071, People's Republic of China
- ³⁸ Peking University, Beijing 100871, People's Republic of China
- ³⁹ Qufu Normal University, Qufu 273165, People's Republic of China
- ⁴⁰ Shandong Normal University, Jinan 250014, People's Republic of China
- ⁴¹ Shandong University, Jinan 250100, People's Republic of China
- ⁴² Shanghai Jiao Tong University, Shanghai 200240, People's Republic of China
- ⁴³ Shanxi Normal University, Linfen 041004, People's Republic of China
- ⁴⁴ Shanxi University, Taiyuan 030006, People's Republic of China
- ⁴⁵ Sichuan University, Chengdu 610064, People's Republic of China
- ⁴⁶ Soochow University, Suzhou 215006, People's Republic of China
- ⁴⁷ Southeast University, Nanjing 211100, People's Republic of China
- ⁴⁸ State Key Laboratory of Particle Detection and Electronics,
Beijing 100049, Hefei 230026, People's Republic of China
- ⁴⁹ Sun Yat-Sen University, Guangzhou 510275, People's Republic of China
- ⁵⁰ Tsinghua University, Beijing 100084, People's Republic of China
- ⁵¹ (A)Ankara University, 06100 Tandogan, Ankara, Turkey; (B)Istanbul Bilgi University, 34060 Eyup, Istanbul, Turkey; (C)Uludag University, 16059 Bursa, Turkey; (D)Near East University, Nicosia, North Cyprus, Mersin 10, Turkey
- ⁵² University of Chinese Academy of Sciences, Beijing 100049, People's Republic of China
- ⁵³ University of Hawaii, Honolulu, Hawaii 96822, USA
- ⁵⁴ University of Jinan, Jinan 250022, People's Republic of China
- ⁵⁵ University of Manchester, Oxford Road, Manchester, M13 9PL, United Kingdom
- ⁵⁶ University of Minnesota, Minneapolis, Minnesota 55455, USA
- ⁵⁷ University of Muenster, Wilhelm-Klemm-Str. 9, 48149 Muenster, Germany
- ⁵⁸ University of Oxford, Keble Rd, Oxford, UK OX13RH
- ⁵⁹ University of Science and Technology Liaoning, Anshan 114051, People's Republic of China
- ⁶⁰ University of Science and Technology of China, Hefei 230026, People's Republic of China
- ⁶¹ University of South China, Hengyang 421001, People's Republic of China
- ⁶² University of the Punjab, Lahore-54590, Pakistan
- ⁶³ (A)University of Turin, I-10125, Turin, Italy; (B)University of Eastern Piedmont, I-15121, Alessandria, Italy; (C)INFN, I-10125, Turin, Italy
- ⁶⁴ Uppsala University, Box 516, SE-75120 Uppsala, Sweden
- ⁶⁵ Wuhan University, Wuhan 430072, People's Republic of China
- ⁶⁶ Xinyang Normal University, Xinyang 464000, People's Republic of China
- ⁶⁷ Zhejiang University, Hangzhou 310027, People's Republic of China
- ⁶⁸ Zhengzhou University, Zhengzhou 450001, People's Republic of China
- ^a Also at Bogazici University, 34342 Istanbul, Turkey
- ^b Also at the Moscow Institute of Physics and Technology, Moscow 141700, Russia
- ^c Also at the Novosibirsk State University, Novosibirsk, 630090, Russia
- ^d Also at the NRC "Kurchatov Institute", PNPI, 188300, Gatchina, Russia
- ^e Also at Istanbul Arel University, 34295 Istanbul, Turkey
- ^f Also at Goethe University Frankfurt, 60323 Frankfurt am Main, Germany
- ^g Also at Key Laboratory for Particle Physics, Astrophysics and Cosmology, Ministry of Education; Shanghai Key Laboratory for Particle Physics and Cosmology; Institute of Nuclear and Particle Physics, Shanghai 200240, People's Republic of China
- ^h Also at Key Laboratory of Nuclear Physics and Ion-beam Application (MOE) and Institute of Modern Physics, Fudan University, Shanghai 200443, People's Republic of China
- ⁱ Also at Harvard University, Department of Physics, Cambridge, MA, 02138, USA
- ^j Currently at: Institute of Physics and Technology, Peace Ave.54B, Ulaanbaatar 13330, Mongolia
- ^k Also at State Key Laboratory of Nuclear Physics and Technology, Peking University, Beijing 100871, People's Republic of China

^l *School of Physics and Electronics, Hunan University, Changsha 410082, China*

By analyzing a data sample corresponding to an integrated luminosity of 2.93 fb^{-1} collected at a center-of-mass energy of 3.773 GeV with the BESIII detector, we measure for the first time the absolute branching fraction of the $D^+ \rightarrow \eta\mu^+\nu_\mu$ decay to be $\mathcal{B}_{D^+ \rightarrow \eta\mu^+\nu_\mu} = (10.4 \pm 1.0_{\text{stat}} \pm 0.5_{\text{syst}}) \times 10^{-4}$. Using the world averaged value of $\mathcal{B}_{D^+ \rightarrow \eta e^+\nu_e}$, the ratio of the two branching fractions is determined to be $\mathcal{B}_{D^+ \rightarrow \eta\mu^+\nu_\mu} / \mathcal{B}_{D^+ \rightarrow \eta e^+\nu_e} = 0.91 \pm 0.13_{(\text{stat}+\text{syst})}$, which agrees with the theoretical expectation of lepton flavor universality within uncertainty. By studying the differential decay rates in five four-momentum transfer intervals, we obtain the product of the hadronic form factor $f_+^\eta(0)$ and the $c \rightarrow d$ Cabibbo-Kobayashi-Maskawa matrix element $|V_{cd}|$ to be $f_+^\eta(0)|V_{cd}| = 0.087 \pm 0.008_{\text{stat}} \pm 0.002_{\text{syst}}$. Taking the input of $|V_{cd}|$ from the global fit in the standard model, we determine $f_+^\eta(0) = 0.39 \pm 0.04_{\text{stat}} \pm 0.01_{\text{syst}}$. On the other hand, using the value of $f_+^\eta(0)$ calculated in theory, we find $|V_{cd}| = 0.242 \pm 0.022_{\text{stat}} \pm 0.006_{\text{syst}} \pm 0.033_{\text{theory}}$.

PACS numbers: 13.20.Fc, 12.15.Hh

In the standard model (SM), the couplings between three families of leptons and gauge bosons are independent of lepton flavors. This property is known as lepton flavor universality (LFU) [1–4]. Semileptonic (SL) decays of pseudoscalar mesons, which are well understood in the SM, offer an ideal platform to test LFU and search for new physics effects. In the past decade, the BaBar, Belle, and LHCb collaborations reported anomalies in LFU tests with various SL B decays. The measured branching fraction (BF) ratios $\mathcal{R}_{\tau/\ell} = \mathcal{B}_{B \rightarrow \bar{D}^{(*)}\tau^+\nu_\tau} / \mathcal{B}_{B \rightarrow \bar{D}^{(*)}\ell^+\nu_\ell}$ ($\ell = \mu, e$) [5–11] deviate from the SM predictions by 3.1σ [12]. Various models [2, 13–17] were proposed to explain these differences. In view of this, scrutinizing the ratios of the semimuonic D decay BFs over their corresponding semielectronic counterparts offers important complementary tests of e - μ LFU. Recently, BESIII reported tests of LFU with the SL decays $D \rightarrow \bar{K}\ell^+\nu_\ell$ [18, 19] and $D \rightarrow \pi\ell^+\nu_\ell$ [20]. Using the world averaged BFs [21], the difference between the BF ratio of $D \rightarrow \pi\ell^+\nu_\ell$ decays which are mediated via $c \rightarrow d\ell^+\nu_\ell$ ($\mathcal{R}_{\mu/e}^{c \rightarrow d} = \mathcal{B}_{D \rightarrow \pi\mu^+\nu_\mu} / \mathcal{B}_{D \rightarrow \pi e^+\nu_e}$) and the SM prediction is below 2σ . Meanwhile, there is still no experimental confirmation of the $D^+ \rightarrow \eta\mu^+\nu_\mu$ decay, although it was predicted in the quark model 30 years ago [22]. Verification of $\mathcal{R}_{\mu/e}^{c \rightarrow d}$ with $D^+ \rightarrow \eta\ell^+\nu_\ell$ decays, which is also mediated via $c \rightarrow d\ell^+\nu_\ell$, is key to clarifying these situations. In this Letter, we report a complementary test of LFU with $D^+ \rightarrow \eta\ell^+\nu_\ell$ decays based on the first measurement of the BF of $D^+ \rightarrow \eta\mu^+\nu_\mu$. Throughout this Letter, charge conjugate channels are always implied. The BF obtained will also be important for the determination of the η - η' mixing angle, which will benefit the understanding of nonperturbative quantum-chromodynamics (QCD) effects [23].

The investigation of $D^+ \rightarrow \eta\mu^+\nu_\mu$ decay dynamics allows the determination of the $c \rightarrow d$ Cabibbo-Kobayashi-Maskawa (CKM) matrix element $|V_{cd}|$ and the hadronic form factor (FF) $f_+^\eta(0)$. The value of $f_+^\eta(0)$ has been calculated with various approaches, e.g., QCD light-cone sum rules (LCSR) [24–26], light-

front quark model (LFQM) [27], covariant confined quark model (CCQM) [28, 29], and relativistic quark model (RQM) [30]. The predicted values vary in a wide range from 0.36 to 0.71. According to Refs. [31, 32], the predicted FFs of the SL D decays are expected to be insensitive to the spectator quark. Measurement of the hadronic FF in $D^+ \rightarrow \eta\mu^+\nu_\mu$ decay can be used to distinguish between these calculations. The predicted FF that passes the experimental test is useful to determine $|V_{cd}|$. Conversely, measurements of SL D decay hadronic FFs help constrain lattice QCD calculations and lead to more reliable calculations of the hadronic FFs of SL D and B decays, which are crucial to accurately determine CKM parameters [31–34], and test the unitarity of the CKM matrix.

In this analysis, we use a data sample corresponding to an integrated luminosity of 2.93 fb^{-1} [35] taken at the center-of-mass energy $\sqrt{s} = 3.773 \text{ GeV}$ with the BESIII detector. Details about the design and performance of the BESIII detector are given in Ref. [36]. Simulated samples produced with the GEANT4-based [37] Monte Carlo (MC) package which includes the geometric description of the BESIII detector and the detector response, are used to determine the detection efficiency and to estimate the backgrounds. The simulation includes the beam energy spread and initial state radiation (ISR) in the e^+e^- annihilations modeled with the generator KKMC [38]. The inclusive MC samples consist of the production of $D^0\bar{D}^0$, D^+D^- , and non- $D\bar{D}$ decays of the $\psi(3770)$, the ISR production of the J/ψ and $\psi(3686)$ states, and the continuum processes incorporated in KKMC [38]. The known decay modes are modeled with EVTGEN [39] using BFs taken from the Particle Data Group [21], and the remaining unknown decays from the charmonium states with LUNDCHARM [40]. The final state radiation from charged particles is incorporated with the PHOTOS package [41]. The vector hadronic FF of the SL decay $D^+ \rightarrow \eta\mu^+\nu_\mu$ is simulated with the modified-pole model [42], where the parameter α of the vector hadronic FF is set to be that of $D^+ \rightarrow \pi^0 e^+\nu_e$ measured by BESIII [43], and the pole

mass is set at the nominal D^{*+} mass [21].

The analysis is performed with the double-tag (DT) method, benefiting from the advantage of D^+D^- pair production at $\sqrt{s} = 3.773$ GeV. If a D^- meson [called single-tag (ST) D^- meson] is fully reconstructed by the hadronic decays $D^- \rightarrow K^+\pi^-\pi^-$, $K_S^0\pi^-$, $K^+\pi^-\pi^-\pi^0$, $K_S^0\pi^-\pi^0$, $K_S^0\pi^+\pi^-\pi^-$, and $K^+K^-\pi^-$, the presence of a D^+ meson is guaranteed. If the $D^+ \rightarrow \eta\mu^+\nu_\mu$ decay can be found in the system recoiling against an ST D^- meson, the candidate event is called a DT event. The BF of the SL decay is determined by

$$\mathcal{B}_{D^+ \rightarrow \eta\mu^+\nu_\mu} = N_{\text{DT}} / (N_{\text{ST}}^{\text{tot}} \cdot \varepsilon_{\text{SL}} \cdot \mathcal{B}_{\eta \rightarrow \gamma\gamma}), \quad (1)$$

where $N_{\text{ST}}^{\text{tot}}$ and N_{DT} are the yields of the ST and DT candidates in data, respectively, and $\mathcal{B}_{\eta \rightarrow \gamma\gamma}$ is the BF of the $\eta \rightarrow \gamma\gamma$ decay. The $\varepsilon_{\text{SL}} = \sum_i [(\varepsilon_{\text{DT}}^i \cdot N_{\text{ST}}^i) / (\varepsilon_{\text{ST}}^i \cdot N_{\text{ST}}^{\text{tot}})]$ is the effective signal efficiency of finding $D^+ \rightarrow \eta\mu^+\nu_\mu$ decay in the presence of the ST D^- meson. Here i denotes the tag mode, and ε_{ST} and ε_{DT} are the efficiencies of selecting the ST and DT candidates, respectively.

This analysis uses the same K^\pm , π^\pm , K_S^0 , γ , and π^0 selection criteria as those employed in Refs. [18, 20, 44–47]. The ST D^- mesons are distinguished from combinatorial backgrounds by using the energy difference $\Delta E \equiv E_{D^-} - E_{\text{beam}}$ and the beam-constrained mass $M_{\text{BC}} \equiv \sqrt{E_{\text{beam}}^2 - |\vec{p}_{D^-}|^2}$. Here, E_{beam} is the beam energy, and E_{D^-} and \vec{p}_{D^-} are the total energy and momentum of the ST D^- candidate in the e^+e^- center-of-mass frame. If multiple combinations for an ST mode are present in an event, the combination with the smallest $|\Delta E|$ per tag mode per charge is retained for further analysis. The candidates are required to satisfy $\Delta E \in (-0.055, 0.045)$ GeV for the tags containing π^0 and $\Delta E \in (-0.025, 0.025)$ GeV for the other tags. For each tag mode, the yield of ST D^- mesons is determined from the maximum likelihood fit of the M_{BC} distribution of the accepted candidates. In the fit, the signal and background are described by an MC-simulated shape and an ARGUS function [48], respectively. To take into account the resolution difference between data and MC simulation, the MC-simulated signal shape is convolved with a double-Gaussian function. The widths and relative abundances of the Gaussian components are free parameters of the fit. The resulting fits of these M_{BC} distributions are exhibited in Fig. 1. The candidates with $M_{\text{BC}} \in (1.863, 1.877)$ GeV/ c^2 are kept for further analysis. The total yield of ST D^- mesons is $N_{\text{ST}}^{\text{tot}} = 1522474 \pm 2125_{\text{stat}}$.

At $\sqrt{s} = 3.773$ GeV, the D^+ and D^- mesons are in back-to-back direction. The $D^+ \rightarrow \eta\mu^+\nu_\mu$ candidates are selected in the sides recoiling against the ST D^- mesons. It is required that there is only one charged track available for muon identification. The muon candidate is required to satisfy $|V_{xy}| < 1$ cm and $|V_z| < 10$ cm, where

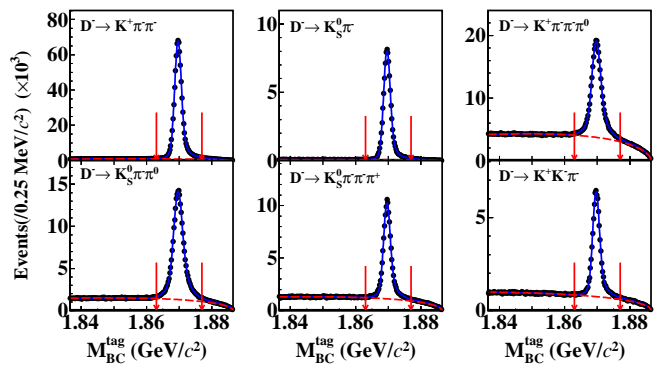


Fig. 1. Fits to the M_{BC} distributions of the ST D^- candidates. Data are shown as dots with error bars. The blue solid and red dashed curves are the fit results and the fitted backgrounds, respectively. Pairs of red arrows show the M_{BC} windows.

$|V_{xy}|$ and $|V_z|$ are the distances of closest approach to the interaction point of the reconstructed track in the transverse plane and along the axis of the drift chamber, respectively. Its polar angle (θ) with respect to the axis of the drift chamber must be within $|\cos\theta| < 0.93$.

Muon identification uses information from the time-of-flight and the electromagnetic calorimeter (EMC), as well as the specific ionization energy loss measured in the main drift chamber. The combined confidence levels for various particle hypotheses (CL_i , $i = e, \mu$, and K) are calculated. Muon candidates are required to satisfy $CL_\mu > 0.001$, $CL_\mu > CL_e$, and $CL_\mu > CL_K$. To reduce misidentification between hadrons and muons, the deposited energy in the EMC of the muon candidate is required to be within (0.105, 0.275) GeV, since it is expected to concentrate around 0.2 GeV.

The η candidates are reconstructed via the $\eta \rightarrow \gamma\gamma$ decay. The invariant mass of the $\gamma\gamma$ candidate is required to be within (0.510, 0.570) GeV/ c^2 . To improve momentum resolution, a one-constraint (1-C) kinematic fit is done on the selected photon pair, whose invariant mass is constrained to the η nominal mass (m_η) [21].

Due to the misidentification of pions as muons, some hadronic D^+ decays survive the above selection criteria. To suppress the peaking backgrounds from $D^+ \rightarrow \eta\pi^+$ decays, we require the $\eta\mu^+$ invariant mass ($M_{\eta\mu^+}$) to be less than 1.74 GeV/ c^2 . To reject the backgrounds containing π^0 , e.g., $D^+ \rightarrow \eta\pi^+\pi^0$, we require that the maximum energy of any extra photon ($E_{\text{extra}}^{\text{max}} \gamma$) is less than 0.30 GeV and there is no extra π^0 ($N_{\text{extra}} \pi^0$) in the candidate event. Here, the extra photon and π^0 denote the ones which have not been used in the DT selection.

The number of SL decays is determined using a kinematic quantity defined as $U_{\text{miss}} \equiv E_{\text{miss}} - |\vec{p}_{\text{miss}}|$, which is expected to peak around 0 for the correctly reconstructed signal events. Here, $E_{\text{miss}} \equiv E_{\text{beam}} - E_\eta - E_{\mu^+}$ and $\vec{p}_{\text{miss}} \equiv \vec{p}_{D^+} - \vec{p}_\eta - \vec{p}_{\mu^+}$ are the missing

energy and momentum of the DT event in the e^+e^- center-of-mass frame, in which $E_{\eta(\mu^+)}$ and $\vec{p}_{\eta(\mu^+)}$ are the energy and momentum of the $\eta(\mu)$ candidates. The U_{miss} resolution is improved by constraining the D^+ energy to the beam energy and $\vec{p}_{D^+} \equiv -\hat{p}_{D^-} \cdot \sqrt{E_{\text{beam}}^2 - m_{D^+}^2}$, where \hat{p}_{D^-} is the unit vector in the momentum direction of the ST D^- and m_{D^+} is the D^+ nominal mass [21].

Figure 2(a) shows the U_{miss} distribution of the accepted DT events in data. The SL decay yield is obtained from an unbinned fit to the U_{miss} distribution, where the SL signal, peaking backgrounds of $D^+ \rightarrow \eta\pi^+\pi^0$, and non-peaking backgrounds (including a small contribution from wrongly reconstructed ST candidates) are described by the corresponding MC-simulated shapes. The yields of the signal and non-peaking backgrounds are free parameters of the fit, while the yield of the peaking background from $D^+ \rightarrow \eta\pi^+\pi^0$ decays is fixed based on MC simulation. The fit result is shown in Fig. 2(a). From the fit, we obtain the yield of DT events $N_{\text{DT}} = 234 \pm 22_{\text{stat}}$. The statistical significance, calculated by $\sqrt{-2\ln(\mathcal{L}_0/\mathcal{L}_{\text{max}})}$, is found to be greater than 10σ . Here, \mathcal{L}_{max} and \mathcal{L}_0 are the maximal likelihood of the nominal fit and that of the fit without signal component, respectively.

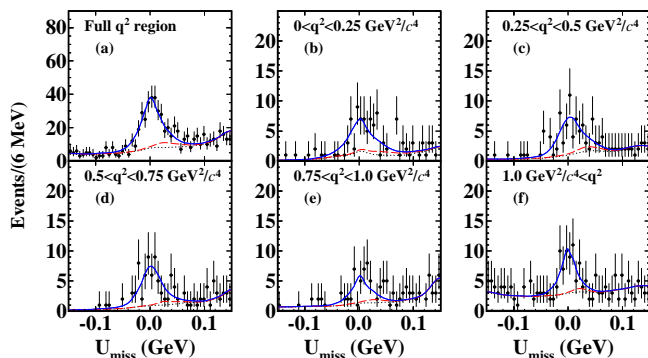


Fig. 2. Fits to the U_{miss} distributions of the $D^+ \rightarrow \eta\mu^+\nu_\mu$ candidate events. Data are shown as dots with error bars. In each figure, the blue solid curve is the fit result, the black dotted curve is the fitted non-peaking background, and the difference between red dashed and black dotted curves is the peaking background of $D^+ \rightarrow \eta\pi^+\pi^0$.

Table 1 of Supplemental Material [49] shows tag dependent numbers of N_{ST}^i , ϵ_{ST}^i , and ϵ_{DT}^i . The average efficiency of detecting $D^+ \rightarrow \eta\mu^+\nu_\mu$ decays is $\epsilon_{\text{SL}} = 0.3752 \pm 0.0013$. Here, the efficiency does not include the BF of the $\eta \rightarrow \gamma\gamma$ decay. To verify the reliability of the efficiency determination, we have compared distributions of momenta and $\cos\theta$ of the η and μ^+ of the selected $D^+ \rightarrow \eta\mu^+\nu_\mu$ candidate events between data and MC simulation, and they are in good agreement.

Inserting N_{DT} , ϵ_{SL} , $N_{\text{ST}}^{\text{tot}}$, and the world average of

$\mathcal{B}_{\eta \rightarrow \gamma\gamma} = 0.3941 \pm 0.0020$ [21] into Eq. (1), we obtain

$$\mathcal{B}_{D^+ \rightarrow \eta\mu^+\nu_\mu} = (10.4 \pm 1.0_{\text{stat}} \pm 0.5_{\text{syst}}) \times 10^{-4}.$$

In the BF measurement, the systematic uncertainties arise from the following sources. The uncertainty in the total yield of ST D^- mesons has been studied in Refs. [18, 20, 44], and is assigned as 0.5%. The muon tracking (PID) efficiencies are studied by analyzing $e^+e^- \rightarrow \gamma\mu^+\mu^-$ events, and the muon tracking (PID) efficiency uncertainty is taken as 0.2% (0.2%) per muon, where the data/MC differences of the two-dimensional (momentum and $\cos\theta$) distributions of the control samples have been re-weighted by those of the $D^+ \rightarrow \eta\mu^+\nu_\mu$ signal decays. The uncertainty of η reconstruction is assumed to be 2.0%, the same as π^0 reconstruction, which was studied with DT $D\bar{D}$ hadronic decays of $D^0 \rightarrow K^-\pi^+$, $K^-\pi^+\pi^+\pi^-$ vs. $\bar{D}^0 \rightarrow K^+\pi^-\pi^0$, $K_S^0\pi^0$ [18, 44]. The uncertainties of the requirements of $E_{\text{extra}}^{\text{max}}$ and $N_{\text{extra}} \pi^0$ are estimated to be 2.3% by analyzing the DT candidate events of $D^+ \rightarrow \eta\pi^+$ and $\pi^0 e^+\nu_e$. The uncertainty due to the $M_{\eta\mu^+}$ requirement is evaluated by replacing the nominal requirement with $M_{\eta\mu^+} < 1.69 \text{ GeV}/c^2$ or $M_{\eta\mu^+} < 1.79 \text{ GeV}/c^2$, and the associated uncertainty is found to be negligible. The uncertainty in the U_{miss} fit is assigned to be 3.7%, which is estimated with alternative signal and background shapes. For alternative background shapes, the uncertainty due to the peaking background of $D^+ \rightarrow \eta\pi^+\pi^0$ has been taken into account via varying the quoted BF by $\pm 1\sigma$. The uncertainty due to the limited MC statistics is 0.5%. The uncertainty in the MC model, 0.3%, is assigned as the difference between our nominal DT efficiency and the DT efficiency determined by re-weighting the q^2 ($q = p_{D^+} - p_\eta$ is the total four momentum of $\mu^+\nu_\mu$) distribution of the signal MC events using the FF parameters obtained from data. Adding these uncertainties quadratically yields the total systematic uncertainty to be 4.9%.

To study the dynamics in $D^+ \rightarrow \eta\mu^+\nu_\mu$ decay, the SL candidate events are divided into five q^2 intervals: (0.0, 0.25), (0.25, 0.5), (0.5, 0.75), (0.75, 1.0), and $(1.0, (m_{D^+} - m_\eta)^2) \text{ GeV}^2/c^4$. The partial decay rate in the i th q^2 interval, $\Delta\Gamma_{\text{measured}}^i$, is determined by

$$\Delta\Gamma_{\text{measured}}^i = N_{\text{produced}}^i / (\tau_{D^+} \cdot N_{\text{ST}}^{\text{tot}}), \quad (2)$$

where N_{produced}^i is the $D^+ \rightarrow \eta\mu^+\nu_\mu$ signal yield produced in the i th q^2 interval in data, τ_{D^+} is the lifetime of D^+ , $N_{\text{ST}}^{\text{tot}}$ is the total yield of ST D^- mesons, and

$$N_{\text{produced}}^i = \sum_j^{N_{\text{intervals}}} (\epsilon^{-1})_{ij} N_{\text{observed}}^j, \quad (3)$$

where N_{observed}^j is the $D^+ \rightarrow \eta\mu^+\nu_\mu$ signal yield observed in the j th q^2 interval and ϵ is the efficiency matrix (Table

2 of Supplemental Material [49]) given by

$$\varepsilon_{ij} = \sum_k \left[(N_{\text{reconstructed}}^{ij} \cdot N_{\text{ST}}) / (N_{\text{generated}}^j \cdot \varepsilon_{\text{ST}}) \right]_k / N_{\text{ST}}^{\text{tot}}. \quad (4)$$

Here, $N_{\text{reconstructed}}^{ij}$ is the $D^+ \rightarrow \eta\mu^+\nu_\mu$ signal yield generated in the j th q^2 interval and reconstructed in the i th q^2 interval, $N_{\text{generated}}^j$ is the total signal yield generated in the j th q^2 interval, and the index k sums over all ST modes.

N_{observed}^i is obtained from the fit to the U_{miss} distribution of the $D^+ \rightarrow \eta\mu^+\nu_\mu$ candidate events in the

$$\Delta\Gamma_{\text{expected}}^i = \int_{q_{\text{min}}^2(i)}^{q_{\text{max}}^2(i)} \left\{ \frac{G_F^2 |V_{cd}|^2}{24\pi^3} \cdot \frac{(q^2 - m_\mu^2)^2 \sqrt{E_\eta^2 - m_\eta^2}}{q^4 m_D^2} \cdot \left[\left(1 + \frac{m_\mu^2}{2q^2} \right) m_D^2 (E_\eta^2 - m_\eta^2) |f_+^\eta(q^2)|^2 \right] \right\} dq^2, \quad (6)$$

where G_F is the Fermi coupling constant; m_μ is the μ^+ mass; $|\vec{p}_\eta|$ and E_η are the momentum and energy of η in the rest frame of D^+ , respectively; the vector hadronic FF $f_+^\eta(q^2)$ is formulated following Ref. [50]. Here, the scalar hadronic FF $f_0^\eta(q^2)$ has been ignored due to negligible sensitivity with limited data.

The FF of $f_+^\eta(q^2)$ can be parameterized by the series expansion [51], which was widely used in previous analyses and verified to be consistent with constraints from QCD [52–54]. Due to limited data, we adopt the two-parameter series expansion form

$$f_+^\eta(q^2) = \frac{f_+^\eta(0)P(0)\Phi(0, t_0)}{P(q^2)\Phi(q^2, t_0)} \cdot \frac{1 + r_1(t_0)z(q^2, t_0)}{1 + r_1(t_0)z(0, t_0)}, \quad (7)$$

where $t_0 = t_+(1 - \sqrt{1 - t_-/t_+})$, $t_\pm = (m_{D^+} \pm m_\eta)^2$, and the functions $P(q^2)$, $\Phi(q^2, t_0)$, and $z(q^2, t_0)$ are defined following Ref. [51].

The statistical covariance matrix is constructed as

$$C_{ij}^{\text{stat}} = \left(\frac{1}{\tau_{D^+} \cdot N_{\text{ST}}^{\text{tot}}} \right)^2 \sum_n \varepsilon_{in}^{-1} \varepsilon_{jn}^{-1} (\sigma(N_{\text{obs}}^n))^2, \quad (8)$$

where n sums from 1 to 5 intervals. The systematic covariance matrix is obtained by summing over that of each systematic uncertainty source, which is taken as

$$C_{ij}^{\text{syst}} = \delta(\Delta\Gamma_{\text{measured}}^i) \delta(\Delta\Gamma_{\text{measured}}^j), \quad (9)$$

where $\delta(\Delta\Gamma_{\text{measured}}^i)$ is the systematic uncertainty of the partial decay rate in the i th q^2 interval. The systematic uncertainties arising from $N_{\text{ST}}^{\text{tot}}$, τ_{D^+} , muon tracking and PID, η reconstruction, as well as $E_{\text{extra}}^{\text{max}} \gamma$ and $N_{\text{extra}} \pi^0$ requirements are taken to be common across all the q^2 intervals; while the others are determined separately in

i th q^2 interval. The fit results of the U_{miss} distributions in various intervals are shown in Figs. 2(b)-(f), and the partial decay rates obtained are shown in Fig. 3.

With the $\Delta\Gamma_{\text{measured}}^i$ obtained above and the partial decay rate $\Delta\Gamma_{\text{expected}}^i$ predicted by theory, the χ^2 is constructed as

$$\chi^2 = \sum_{i,j=1}^5 (\Delta\Gamma_{\text{measured}}^i - \Delta\Gamma_{\text{expected}}^i) C_{ij}^{-1} (\Delta\Gamma_{\text{measured}}^j - \Delta\Gamma_{\text{expected}}^j), \quad (5)$$

where $C_{ij} = C_{ij}^{\text{stat}} + C_{ij}^{\text{syst}}$ is the covariance matrix of the measured partial decay rates among q^2 intervals, and

each q^2 interval as above.

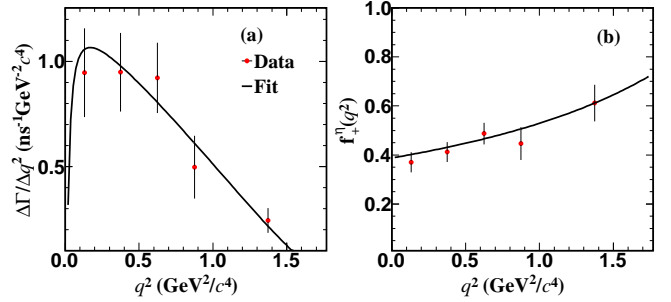


Fig. 3. (a) Fit to the partial decay rates and (b) projection to $f_+^\eta(q^2)$ for $D^+ \rightarrow \eta\mu^+\nu_\mu$. Dots with error bars are data, and the solid curves are the fit results.

Minimizing the χ^2 in Eq. (5) gives the product of $f_+^\eta(0)|V_{cd}|$ and the first order coefficient r_1 to be $0.087 \pm 0.008_{\text{stat}} \pm 0.002_{\text{syst}}$ and $-0.9 \pm 2.7_{\text{stat}} \pm 0.2_{\text{syst}}$, respectively. The nominal fit parameters are taken from the fit with the combined statistical and systematic covariance matrix, and their statistical uncertainties are taken from the fit only with the statistical covariance matrix. For each parameter, the systematic uncertainty is obtained by calculating the quadratic difference of uncertainties between these two fits. The fit result is shown in Fig. 3 and the goodness-of-fit is $\chi^2/\text{NDOF} = 1.0/3$, where NDOF is the number of degrees of freedom. The $f_+^\eta(0)|V_{cd}|$ measured in this work is consistent with the measurements using $D^+ \rightarrow \eta e^+\nu_e$ by CLEO [55] and BESIII [56].

Using our product of $f_+^\eta(0)|V_{cd}|$ and the $f_+^\eta(0)$ calculated in Ref. [29] leads to $|V_{cd}| = 0.242 \pm 0.022_{\text{stat}} \pm 0.006_{\text{syst}} \pm 0.033_{\text{theory}}$. This result is consistent with our

previous measurements of $|V_{cd}|$ via $D^+ \rightarrow \ell^+ \nu_\ell$ [60, 61] and $D^{0(+)} \rightarrow \pi^{-(0)} e^+ \nu_e$ [43, 54]. Conversely, using our product of $f_+^\eta(0)|V_{cd}|$ and the $|V_{cd}| = 0.22438 \pm 0.00044$ given by CKMFitter [21] yields $f_+^\eta(0) = 0.39 \pm 0.04_{\text{stat}} \pm 0.01_{\text{syst}}$. Table 1 shows comparison of our BF and hadronic FF with various theoretical calculations for $D^+ \rightarrow \eta \ell^+ \nu_\ell$. Our BF result disfavors the prediction in Ref. [26] by 2.6σ but agrees with the other predictions [24, 25, 28, 30, 57] within 1.5σ . Our result for $f_+^\eta(0)$ agrees well with the predictions in Refs. [25, 29]. However, it clearly rules out the prediction in Ref. [27], and disfavors the predictions in Refs. [24, 26, 28, 30] by about 2.4 - 3.8σ . Using our $f_+^\eta(0)$ and the world average of $f_+^\pi(0) = 0.6351 \pm 0.0081$ [12], we determine the hadronic FF ratio to be $f_+^\eta(0)/f_+^\pi(0) = 0.61 \pm 0.06_{\text{stat}} \pm 0.02_{\text{syst}}$. This provides a valuable constraint to improve the calculations of these hadronic FFs in lattice QCD.

In summary, the SL decay $D^+ \rightarrow \eta \mu^+ \nu_\mu$ has been observed by analyzing 2.93 fb^{-1} of data collected at $\sqrt{s} = 3.773 \text{ GeV}$. The absolute BF of this decay is determined for the first time to be $\mathcal{B}_{D^+ \rightarrow \eta \mu^+ \nu_\mu} = (10.4 \pm 1.0_{\text{stat}} \pm 0.5_{\text{syst}}) \times 10^{-4}$. Using the world averaged value of $\mathcal{B}_{D^+ \rightarrow \eta e^+ \nu_e} = (11.4 \pm 1.0) \times 10^{-4}$ gives the BF ratio $R_{\mu/e} = \mathcal{B}_{D^+ \rightarrow \eta \mu^+ \nu_\mu} / \mathcal{B}_{D^+ \rightarrow \eta e^+ \nu_e} = 0.91 \pm 0.13$, where the uncertainty is the sum in quadrature of the statistical and systematic errors, but dominated by the statistical error. This result agrees with the SM predictions (0.97-1.00) [24, 29, 57], thereby implying no LFU violation within current sensitivity. The obtained BF can be used to determine the η - η' mixing angle once $\mathcal{B}_{D^+ \rightarrow \eta' \mu^+ \nu_\mu}$ is measured with large data samples [58, 59] in the near future. By analyzing the dynamics of $D^+ \rightarrow \eta \mu^+ \nu_\mu$ decay, the product of $f_+^\eta(0)|V_{cd}|$ has been determined to be $0.087 \pm 0.008_{\text{stat}} \pm 0.002_{\text{syst}}$. Combining necessary inputs, we have obtained $f_+^\eta(0) = 0.39 \pm 0.04_{\text{stat}} \pm 0.01_{\text{syst}}$ and $|V_{cd}| = 0.242 \pm 0.022_{\text{stat}} \pm 0.006_{\text{syst}} \pm 0.033_{\text{theory}}$. The obtained $f_+^\eta(0)$ provides important data to test various theoretical calculations, while the obtained $|V_{cd}|$ is valuable for the CKM matrix unitarity test.

The BESIII collaboration thanks the staff of BEPCII and the IHEP computing center for their strong support. This work is supported in part by National Key Basic Research Program of China under Contract No. 2015CB856700; National Natural Science Foundation of China (NSFC) under Contracts Nos. 11775230, 11475123, 11625523, 11635010, 11735014, 11822506, 11835012, 11935015, 11935016, 11935018, 11961141012; the Chinese Academy of Sciences (CAS) Large-Scale Scientific Facility Program; Joint Large-Scale Scientific Facility Funds of the NSFC and CAS under Contracts Nos. U1532101, U1932102, U1732263, U1832207; CAS Key Research Program of Frontier Sciences under Contracts Nos. QYZDJ-SSW-SLH003, QYZDJ-SSW-SLH040; 100 Talents Program of CAS; INPAC and Shanghai Key Laboratory for Particle Physics and Cosmology; ERC under Contract No. 758462;

German Research Foundation DFG under Contracts Nos. Collaborative Research Center CRC 1044, FOR 2359; Istituto Nazionale di Fisica Nucleare, Italy; Ministry of Development of Turkey under Contract No. DPT2006K-120470; National Science and Technology fund; STFC (United Kingdom); The Knut and Alice Wallenberg Foundation (Sweden) under Contract No. 2016.0157; The Royal Society, UK under Contracts Nos. DH140054, DH160214; The Swedish Research Council; U. S. Department of Energy under Contracts Nos. DE-FG02-05ER41374, DE-SC-0012069.

-
- [1] A. Salam and J. C. Ward, Phys. Lett. **13**, 168 (1964).
 - [2] S. Fajfer, J. F. Kamenik, I. Nisandzic, and U. Rojcek, Phys. Rev. Lett. **109**, 161801 (2012).
 - [3] S. Fajfer, I. Nisandzic, and U. Rojcek, Phys. Rev. D **91**, 094009 (2015).
 - [4] X. D. Guo, X. Q. Hao, H. W. Ke, M. G. Zhao, and X. Q. Li, Chin. Phys. C **41**, 093107 (2017).
 - [5] J. P. Lees *et al.* (BaBar Collaboration), Phys. Rev. Lett. **109**, 101802 (2012).
 - [6] J. P. Lees *et al.* (BaBar Collaboration), Phys. Rev. D **88**, 072012 (2013).
 - [7] R. Aaij *et al.* (LHCb Collaboration), Phys. Rev. Lett. **115**, 111803 (2015).
 - [8] M. Huschle *et al.* (Belle Collaboration), Phys. Rev. D **92**, 072014 (2015).
 - [9] Y. Sato *et al.* (Belle Collaboration), Phys. Rev. D **94**, 072007 (2016).
 - [10] R. Aaij *et al.* (LHCb Collaboration), Phys. Rev. D **97**, 072013 (2018).
 - [11] A. Abdesselam *et al.* (Belle Collaboration), arXiv: 1904.08794 [hep-ex].
 - [12] Y. Amhis *et al.* (Heavy Flavor Averaging Group), arXiv:1909.12524 [hep-ex].
 - [13] S. Fajfer, J. F. Kamenik, and I. Nisandzic, Phys. Rev. D **85**, 094025 (2012).
 - [14] A. Celis *et al.*, J. High Energy Phys. **1301**, 054 (2013).
 - [15] A. Crivellin, G. D'Ambrosio and J. Heeck, Phys. Rev. Lett. **114**, 151801 (2015).
 - [16] A. Crivellin, J. Heeck, and P. Stoffer, Phys. Rev. Lett. **116**, 081801 (2016).
 - [17] M. Bauer and M. Neubert, Phys. Rev. Lett. **116**, 141802 (2016).
 - [18] M. Ablikim *et al.* (BESIII Collaboration), Eur. Phys. J. C **76**, 369 (2016).
 - [19] M. Ablikim *et al.* (BESIII Collaboration), Phys. Rev. Lett. **122**, 011804 (2019).
 - [20] M. Ablikim *et al.* (BESIII Collaboration), Phys. Rev. Lett. **121**, 171803 (2018).
 - [21] M. Tanabashi *et al.* (Particle Data Group), Phys. Rev. D **98**, 030001 (2018) and 2019 update.
 - [22] N. Isgur, D. Scora, B. Grinstein, and M. B. Wise, Phys. Rev. D **39**, 799 (1989).
 - [23] C. D. Donato, G. Ricciardi, and I. Bigi, Phys. Rev. D **85**, 013016 (2012).
 - [24] Y. L. Wu, M. Zhong, and Y. B. Zuo, Int. J. Mod. Phys. A **21**, 6125 (2006).
 - [25] G. Duplancic and B. Melic,

Table 1. Comparison of our BF (in $\times 10^{-4}$) and hadronic FF with various theoretical calculations for $D^+ \rightarrow \eta \ell^+ \nu_\ell$. The first and second uncertainties are statistical and systematic, respectively. Theoretical calculations listed in the table assume no gluon component for η' . Numbers marked with * denote that the predicted $\mathcal{B}_{D^+ \rightarrow \eta e^+ \nu_e}$ is listed due to no predictions for $D^+ \rightarrow \eta \mu^+ \nu_\mu$ in Refs. [25, 26].

	This work	LCSR [24]	LCSR [25]	LCSR [26]	LFQM [27]	CLFQM [57]	CCQM [28]	CCQM [29]	RQM [30]
$\mathcal{B}_{D^+ \rightarrow \eta \mu^+ \nu_\mu}$	$10.4 \pm 1.0 \pm 0.5$	$8.4^{+1.6}_{-1.4}$	$14 \pm 11^*$	$24.5 \pm 5.3^*$...	12 ± 1	9.12	...	12.1
Difference (σ)	...	1.0	0.3	2.6	...	1.1	1.1	...	1.5
$f_+^\eta(0)$	$0.39 \pm 0.04 \pm 0.01$	$0.56^{+0.06}_{-0.05}$	$0.43^{+0.17}_{-0.14}$	0.55 ± 0.05	0.71 ± 0.01	...	0.67 ± 0.11	0.36 ± 0.05	0.547
Difference (σ)	...	2.5	0.3	2.5	7.5	...	2.4	0.5	3.8

- J. High Energy Phys. **1511**, 138 (2015).
- [26] N. Offen, F. A. Porkert, and A. Schafer, Phys. Rev. D **88**, 034023 (2013).
- [27] R. C. Verma, J. Phys. G **39**, 025005 (2012).
- [28] N. R. Soni, M. A. Ivanov, J. G. Körner, J. N. Pandya, P. Santorelli, and C. T. Tran, Phys. Rev. D **98**, 114031 (2018).
- [29] M. A. Ivanov, J. G. Körner, J. N. Pandya, P. Santorelli, N. R. Soni, and C. T. Tran, Front. Phys. (Beijing) **14**, 64401 (2019).
- [30] R. N. Faustov, V. O. Galkin, and X. W. Kang, Phys. Rev. D **101**, 013004 (2020).
- [31] J. Koponen, C. T. H. Davies, and G. Donald (HPQCD Collaboration), arXiv:1208.6242[hep-lat].
- [32] J. Koponen, C. T. H. Davies, G. C. Donald, E. Follana, G. P. Lepage, H. Na, and J. Shigemitsu (HPQCD Collaboration), arXiv:1305.1462[hep-lat].
- [33] N. Brambilla *et al.*, Eur. Phys. J. C **74**, 2981 (2014).
- [34] J. A. Bailey *et al.* (Fermilab Lattice and MILC Collaborations), Phys. Rev. D **85**, 114502 (2012); Erratum: Phys. Rev. D **86**, 039904 (2012).
- [35] M. Ablikim *et al.* (BESIII Collaboration), Chin. Phys. C **37**, 123001 (2013); Phys. Lett. B **753**, 629 (2016).
- [36] M. Ablikim *et al.* (BESIII Collaboration), Nucl. Instr. Method A **614**, 345 (2010).
- [37] S. Agostinelli *et al.* (GEANT4 Collaboration), Nucl. Instr. Method A **506**, 250 (2003).
- [38] S. Jadach, B. F. L. Ward, and Z. Was, Phys. Rev. D **63**, 113009 (2001); Comput. Phys. Commun. **130**, 260 (2000).
- [39] D. J. Lange, Nucl. Instrum. Meth. A **462**, 152 (2001); R. G. Ping, Chin. Phys. C **32**, 599 (2008).
- [40] J. C. Chen, G. S. Huang, X. R. Qi, D. H. Zhang, and Y. S. Zhu, Phys. Rev. D **62**, 034003 (2000).
- [41] E. Richter-Was, Phys. Lett. B **303**, 163 (1993).
- [42] D. Becirevic and A. B. Kaidalov, Phys. Lett. B **478**, 417 (2000).
- [43] M. Ablikim *et al.* (BESIII Collaboration), Phys. Rev. D **96**, 012002 (2015).
- [44] M. Ablikim *et al.* (BESIII Collaboration), Chin. Phys. C **40**, 113001 (2016).
- [45] M. Ablikim *et al.* (BESIII Collaboration), Phys. Rev. Lett. **123**, 231801 (2019).
- [46] M. Ablikim *et al.* (BESIII Collaboration), Phys. Rev. D **101**, 052009 (2020).
- [47] M. Ablikim *et al.* (BESIII Collaboration), Phys. Rev. D **101**, 072005 (2020).
- [48] H. Albrecht *et al.* (ARGUS Collaboration), Phys. Lett. B **241**, 278 (1990).
- [49] See Supplemental Material for tag dependent ST yields in data, ST efficiencies, DT efficiencies, and signal efficiencies of $D^+ \rightarrow \eta \mu^+ \nu_\mu$, as well as the efficiency matrix of $D^+ \rightarrow \eta \mu^+ \nu_\mu$ across different q^2 intervals.
- [50] J. G. Körner and G. A. Schuler, Z. Phys. C **46**, 93 (1990).
- [51] T. Becher and R. J. Hill, Phys. Lett. B **633**, 61 (2006).
- [52] D. Besson *et al.* (CLEO Collaboration), Phys. Rev. D **80**, 032005 (2009).
- [53] J. P. Lees *et al.* (BaBar Collaboration), Phys. Rev. D **91**, 052002 (2015).
- [54] M. Ablikim *et al.* (BESIII Collaboration), Phys. Rev. D **92**, 072012 (2015).
- [55] S. Dobbs *et al.* (CLEO Collaboration), Phys. Rev. D **84**, 032001 (2011).
- [56] M. Ablikim *et al.* (BESIII Collaboration), Phys. Rev. D **97**, 092009 (2018).
- [57] H. Y. Cheng and X. W. Kang, Eur. Phys. J. C **77**, 587 (2017); Erratum: Eur. Phys. J. C **77**, 863 (2017).
- [58] M. Ablikim *et al.* (BESIII Collaboration), Chin. Phys. C **44**, 040001 (2020).
- [59] E. Kou *et al.* (Belle II Collaboration), PTEP **2019**, 123C01 (2019).
- [60] M. Ablikim *et al.* (BESIII Collaboration), Phys. Rev. D **89**, 051104 (2014).
- [61] M. Ablikim *et al.* (BESIII Collaboration), Phys. Rev. Lett. **123**, 211802 (2019).

SUPPLEMENTAL MATERIAL

Table 1 shows the tag dependent ST yields in data, ST efficiencies, DT efficiencies, and signal efficiencies of $D^+ \rightarrow \eta\mu^+\nu_\mu$. Table 2 shows the efficiency matrix of $D^+ \rightarrow \eta\mu^+\nu_\mu$ across different q^2 intervals averaged over six tag modes.

Table 1. Tag dependent ST yields in data, ST efficiencies, DT efficiencies and signal efficiencies of $D^+ \rightarrow \eta\mu^+\nu_\mu$. The efficiencies do not include the BF's of K_S^0 , π^0 , and η . The uncertainties are statistical only.

ST mode	N_{ST}	ϵ_{ST} (%)	ϵ_{DT} (%)	$\epsilon_{\eta\mu\nu} = \epsilon_{\text{DT}}/\epsilon_{\text{ST}}$ (%)
$K^+\pi^-\pi^-$	782669 ± 990	50.57 ± 0.06	19.00 ± 0.09	37.23 ± 0.18
$K^+\pi^-\pi^-\pi^0$	251008 ± 1135	26.72 ± 0.09	9.71 ± 0.08	36.02 ± 0.33
$K_S^0\pi^-$	91345 ± 320	50.39 ± 0.17	20.56 ± 0.11	40.44 ± 0.25
$K_S^0\pi^-\pi^0$	215364 ± 1238	27.25 ± 0.07	11.41 ± 0.12	41.49 ± 0.45
$K_S^0\pi^+\pi^-\pi^-$	113054 ± 889	28.29 ± 0.12	10.15 ± 0.18	35.54 ± 0.64
$K^+K^-\pi^-$	69034 ± 460	40.87 ± 0.24	13.66 ± 0.10	33.13 ± 0.32

Table 2. Efficiency matrix (%) of $D^+ \rightarrow \eta\mu^+\nu_\mu$ across different q^2 intervals.

ϵ_{ij}	1	2	3	4	5
1	34.99	1.10	0.01	0.00	0.00
2	1.19	34.40	1.66	0.00	0.00
3	0.03	1.53	34.78	2.12	0.01
4	0.02	0.04	1.67	34.49	1.58
5	0.02	0.04	0.07	1.86	36.53